

**Achievement of acoustical properties of foam materials by tuning
membrane level:**

Elaborations, Models and Experiments

V.H. Trinh^a and C. Perrot*

*Laboratoire Modélisation et Simulation Multi Echelle,
MSME UMR 8208 CNRS, Université Paris-Est, Marne-la-Vallée, France*

V. Langlois

*Laboratoire Géomatériaux et Environnement, LGE EA 4508,
77454, Université Paris-Est, Marne-la-Vallée, France*

O. Pitois and Y. Khidas

*Laboratoire Navier, NAVIER UMR 8205 CNRS,
MSME UMR 8208 CNRS, Université Paris-Est, Marne-la-Vallée, France*

(Dated: December 12, 2017)

arXiv:1712.03849v1 [physics.app-ph] 11 Dec 2017

^aAlso at Le Quy Don Technical University, Hanoi, Vietnam

Abstract

This work presents a combined numerical and experimental approach to characterize the macroscopic transport and acoustic behavior of foam materials with a membrane cellular structure. A direct link between the sound absorption behavior of a membrane foam-based layer and its local microstructural morphology is also investigated. To this regard, we first produce a set of foam samples having the same density and the same monodisperse pore size but different values of the closure rate of the windows separating the foam pores. Then, the morphology of pore connectivity with membranes is measured directly on SEM together binocular images. The obtained morphological information is used to reconstruct the representative unit cell for computational performance. The knowledge of the computational model of acoustic porous materials obtained by a hybrid approach based on the scaling laws and the semi-phenomenological JCAL model. For validation purpose, the numerical simulations are further compared with the experimental data obtained from a set of three-microphone tube tests, a very good agreement is observed. In acoustic terms, the obtained results point out that for the given high porosity and cell size, we can archive a high sound absorbing ability of based-foam layer by controlling the membrane level at a range of 45-85%. To elaborate these foams, a gelatin concentration in a range of 14-18% should be used in the foam making process. In addition, we can obtain for instance the peak and the average values of acoustic absorption of a foam layer in a specific frequency range of interest by varying its membrane content. Methodologically, our work proposes (i) a systematic approach to characterize directly macroscopic properties from the local microstructure, and (ii) a manufacturing technique that can be used to make foams with the desired microstructure.

PACS numbers: PACS: XXXX

* camille.perrot@u-pem.fr; Corresponding author.

I. INTRODUCTION

Noise reduction is of particular concern in many fields, for instance, automotive, aeronautical, and construction industries. Hence, the design task of acoustical materials has recently gained popularity in both academic science and industry. One promising way to solve this task is through the design and optimization of porous structures at some relevant scales. The acoustical macro-behavior of porous materials has been modeled from their microstructure by different methods [6–10] for a wide range of porous structures [1–5]. From knowledge about the above micro-macro link, by varying the local geometry of porous materials, several works have focused on defining the optimal microstructure for the target of sound absorption capability [15–17].

The rigid-frame porous material assumption is still widely adopted to treat sound absorbing property applications in which the elastic properties of the skeleton do not play a significant role. Two main numerical methods introduced below takes into account only the motions of the fluid phase.

A hybrid method relies on approximate but robust semi-phenomenological model named in the literature as JCAL (Johnson-Champoux-Allard-Lafarge) model [11–13]. This model derives the visco-inertial and thermal effects from macroscopic parameters with the principle is to solve the local equations governing the asymptotic frequency-dependent visco-thermal dissipation phenomena at the microscopic scale. All the macroscopic parameters of interest can be determined from only three asymptotic calculations (based on the steady Stokes, Laplace, and diffusion-controlled reaction equations) and the frequency-dependent description reconstructed. Contrary, a direct approach solves the linearized Navier-Stokes and the heat equations in harmonic regime in each studied frequency. These parameters allowed use the approximation formulas for the frequency-dependent effective density and effective compressibility [1, 14]. It should be noted that in comparison with the hybrid method the direct approach requires a computational cost by computations of each frequency, especially for cases of complex structure or larger number of computational configurations. For all mentioned above, this work follows up the hybrid framework to model the sound propagation in membrane foams.

Acoustic performance of cellular polymer foams was investigated by various works for both open cell and closed cell structures [18–22]. To this regard, it has been shown that

foam membranes, i.e. the solid films closing the windows separating the foam pores, can be of primary importance in acoustical capacity whereas they may occupy a very small volume fraction within the material. Accounting for the membranes effect led to the introduction of dedicated parameters, by measuring simply the fraction of open windows [10, 19, 23] or distinguishing both fully open and partially open windows [18, 24–28]. From such a refined microstructural description, the homogenization method was found to predict successfully the acoustic properties of several polyurethane foam samples [18, 27, 28].

However, a complete validation of such method would require considering a set of foam samples allowing for the membrane parameter to be varied within a significant range of values. In this study, we elaborate polymer foam samples showing several membrane contents. The classical numerical homogenization method based on the local geometry models of these real membrane foams is employed to calculate the macroscopic transport properties. The sound absorption performance of foam layers is derived from these values using the JCAL model [11–13]. The numerical results show a good agreement with the measured data using a three-microphone impedance tube. In the end of this work, a systematic micro-macro link is investigated based on our proposed numerical approach. Additionally, some suggestions are also provided to the existing methods, which are used to predict sound absorbing behavior of the partially open cell foams within large range of membrane level.

The remaining part of this paper is organized as follows. Sec. II deals with a brief introduction of the hybrid numerical approach based on the idealized representative unit cell for defining the link between microstructure and properties of acoustic materials. Sec. III is devoted the experimental validation involving foam manufacturing process as well as property characterizations of foam sample. In Sec. IV, computed results are first further compared with measurements, then some comments in terms of modeling membrane cellular foams are then provided. Finally, in Sec. V, we conclude this research and provide directions for future work.

II. NUMERICAL METHOD

A. Equivalent fluid of porous materials

From the macroscopic perspective, the equivalent-fluid approach is applied where a rigid porous medium is substituted by an effective fluid. This fluid is characterized by the effective density [11] and effective bulk modulus [12, 13] as follows:

$$\rho(\omega) = \frac{\rho_0}{\phi} \left[\alpha_\infty + \frac{\phi\sigma}{j\omega\rho_0} \sqrt{1 + j\omega\frac{\rho_0}{\eta} \left(\frac{2\eta\alpha_\infty}{\sigma\phi\Lambda} \right)^2} \right] \quad (1)$$

and

$$K(\omega) = \frac{\gamma P_0 / \phi}{\gamma - (\gamma - 1) \left[1 - j \frac{\phi\kappa}{k'_0 C_p \rho_0 \omega} \sqrt{1 + j \frac{4k'_0 P_0 \rho_0 \omega}{\kappa \Lambda^2 \phi^2}} \right]^{-1}} \quad (2)$$

in which ρ_0 and η denote the density and dynamic viscosity of the ambient fluid (i.e. air). $\kappa = \gamma P_0$ is the air adiabatic bulk modulus, P_0 the atmospheric pressure, and $\gamma = C_p / C_v$ is the ratio of heat capacity at constant pressure (C_p) to the heat capacity at constant volume (C_v).

The JCAL effective fluid model involves 6 macroscopic parameters (ϕ , Λ' , σ , α_∞ , Λ , k'_0) in order to describe visco-inertial as well as thermal dissipative effects inside the porous media. In which, the porosity ϕ and thermal characteristic length Λ are defined directly from the local geometry, and others are computed from numerical solutions of (i) the Stoke equations [11] (the static air flow resistivity σ); (ii) the inertial equations [11] (the high frequency tortuosity α_∞ and the viscous characteristic length Λ') and (iii) the diffusion equations [29] (for the static permeability k'_0), (detailed view see [20] and Appendix A).

In acoustic terms, a homogeneous layer is described by the wave number $k_c(\omega)$ and the characteristic impedance $Z_c(\omega)$ as follow [48],

$$k_c(\omega) = \omega \sqrt{\rho(\omega) / K(\omega)}, \quad Z_c(\omega) = \sqrt{\rho(\omega) K(\omega)} \quad (3)$$

The normal incidence sound absorption coefficient of this porous layer is derived from the

complex reflection factor by,

$$\alpha = 1 - \left| \frac{Z_s(\omega) - Z_0}{Z_s(\omega) + Z_0} \right|^2 \quad (4)$$

with Z_0 is the air impedance and $Z_s(\omega)$ is the normal incidence surface impedance. For a layer of thickness L_s , $Z_s(\omega)$ is given as, $Z_s(\omega) = -jZ_c(\omega)\cot(k_c(\omega)L_s)$.

B. Representative unit cell of foams

The idealized Kelvin’s tetrakaidecahedron is widely used for modeling high porous foams [30]. This space-filling arrangement of idelical cell is a good presentative structure for real cellular foams with equal-sized bubbles or cells of equal volume [7]. The cross section of struts of this framework is modeled in different shapes such as circle, triangular or concave shape, interestingly, the ligament shape has limited influence on macroscopic acoustic properties [19, 20], it means that we can able to treat this shape in simple one (i.e. triangular). A periodic unit cell (PUC) is used to represent the local structure of our foam samples (see an unit cell (Fig. (2.e)) and the corresponding finite element mesh (Fig. 2(f)). The cell is based on an order packing of 14-sided polyhedron with 6 squared faces and 8 hexagonal faces. As we are mostly interested in the effect of the closure rate of windows, the cell skeleton is made of idealized ligament having a length and an equilateral triangular cross section of edge side (see Appendix D). For PUC in a case of membrane closed cell structure, the morphology of films in window faces of material framework will be characterized corresponding to local property of membrane in the next section (for more details, see Sec. III B and Supplemental material).

III. EXPERIMENTAL VALIDATION

A. Elaboration of controlled polymer foams

We elaborate solid polymer foam samples having a gas volume fraction ϕ and a monodisperse pore size D_b , but a tunable membrane content. The foam making procedure can be described as follows (see Fig. 1):

(1) Monodisperse precursor aqueous foam is generated. Foaming liquid, i.e. TTAB at 3 g/L in water, and nitrogen are pushed through a T-junction allowing controlling the bubble

size by adjusting the flow rate of each fluid. Produced bubbles are stored in a glass column and a constant liquid fraction over the foam column is set at 0.99 by imbibition from the top with foaming solution.

(2) An aqueous gelatin solution is prepared at a mass concentration C_{gel} within the range 12-18%. The temperature of this solution is maintained at $T \approx 60^\circ\text{C}$ in order to remain above the sol/gel transition (30°C).

(3) The precursor foam and the hot gelatin solution are mixed in a continuous process thanks to a mixing device based on flow-focusing method [32]. By tuning the flow rates of both the foam and the solution during the mixing step, the gas volume fraction can be set, $= 0.8$. Note also that the bubble size is conserved during the mixing step. The resulting foamy gelatin is continuously poured into a cylindrical cell (diameter: 40 mm and height: 40 mm) which is rotating around its axis of symmetry at approximately 50 rpm. This process allows for gravity effects to be compensated until the temperature decreases below the setting temperature.

(4) The cell is let one hour at 0°C , then one week in a climatic chamber ($T = 20^\circ\text{C}$ and $\text{RH} = 30\%$). During that stay, water evaporates from the samples and the gas fraction increases significantly.

(5) After unmolding, a slice (thickness: 20 mm and diameter: 40 mm) is cut (see Fig. 3(c)).

B. Characterization of the foam samples

As a density of the dried gelatin was measured to be 1.36 kg/m^3 , the volume and weight measurements of the prepared samples give values of pore volume fraction. For the gelatin concentrations used in this study, the pore volume fraction was found to vary between 0.977 and 0.983, so that in the following we will consider that this parameter is approximately constant and equal to 0.980 ± 0.003 . Observation of the cylindrical surface of the sample (see Fig. 2(a) allows for the pore (bubble) size to be measured: $= 810 \mu\text{m}$ (the absolute error on is $\pm 30 \mu\text{m}$) for all samples. In addition, the shape anisotropy degree was estimated through a ratio as (see Fig. 2(b)), note that this degree is also considered in both axial and radial directions), providing values smaller than 1.15 for all samples, which justify to neglect this effect in the following. The membrane content is evaluated by measuring the

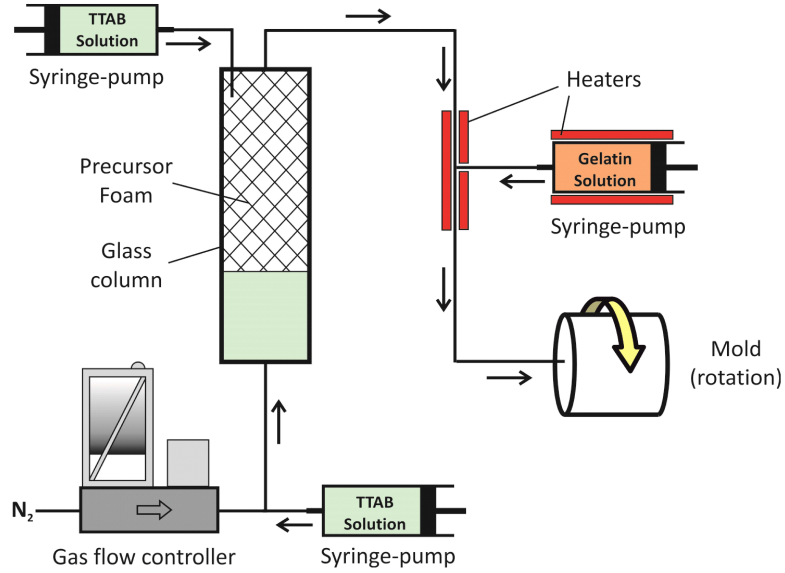


FIG. 1. (Color online) Diagram of foam making process

closure rate of windows separating the pores. We proceed as follows: over several hundred windows observed on both the top and bottom sample surfaces, the proportion of fully closed windows x_{fc} is measured. For the partially closed windows x_p , with a proportion equal to $(1-x_{fc})$, their average closure degree is also measured: $r_c = 1 - \sqrt{A_{elip}/A_{poly}}$, where A_{poly} is the window area (the area of the corresponding polygonal face) and A_{elip} is the aperture area (the area of the fitting ellipse with the aperture) (see Fig. 2(c)). According to these notations, the membrane closed fraction writes: Note that in order to get all the structural information required for the modeling (for PUC mentioned previously), we refine this treatment by distinguishing the windows counting 4 or less edges (referred to as 'sq'), from the windows counting more than 4 edges (referred to as 'hex'). The global closure rate of the cell can be tuned by varying the number of partially closed windows, i.e. and as well as the closure level of those windows, i.e. r^{sq} and r^{hex} respectively. The number of fully closed windows is equal to: $N_{fc}^{sq} = 6 - N_p^{sq}$, $N_{fc}^{hex} = 8 - N_p^{hex}$.

The structural characterization was completed by a measurement of the membrane thickness through SEM microscopy (Fig. 2(d)). From ten SEM images we obtain an average thickness equal to $1.5 \pm 0.25 \mu\text{m}$, which is close to thicknesses measured for similar polymer foams [18, 24, 27].

The static resistivity σ of foam samples is obtained from the measured differential pres-

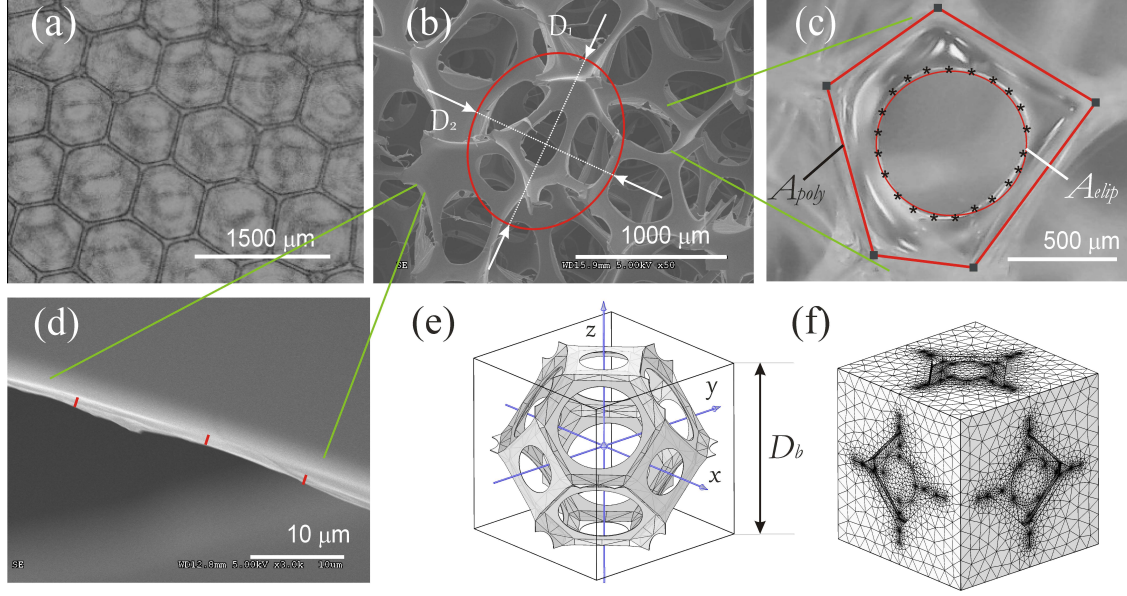


FIG. 2. (Color online) Characterizations of dried-gelatin foams materials: top view of foam sample (a), anisotropy degree (b, membrane closure rate (c), and membrane thickness (d) measurements, an unit cell (e) and its finite element mesh (f).

tures Δp and the controlled steady laminar flow rate Q [33], according to the standard ISO 9053 (method A): $\sigma = \Delta p A_s / Q L_s$ with A_s and L_s are the cross-section area and thickness of sample, $A_s = 12.57 \text{ cm}^2$, $L_s = 20 \text{ mm}$. The relative error of this measure is lower than 10%.

Acoustic properties are determined with a 3-microphone impedance tube [34, 35] (length: 1 m, diameter: 40 mm) (see Fig. 3(a)). Separating distances are as: Micro. #1-Micro. #2: $d_{12} = 35 \text{ mm}$, Micro. #2-Sample: $d_{2s} = 80 \text{ mm}$, and Sample-Micro. #3: 0 mm (Fig. 3(b)). It is kept in mind that the diameter of the samples was slightly larger than 40 mm so that air leakage issue and sample vibration were successfully avoided. The test frequency ranges from 4 Hz to 4500 Hz with a step size of 4 Hz.

IV. RESULTS AND DISCUSSION

A. Non-acoustic property

As presented in Table I, it can be revealed that the gelatin concentration C_{gel} (varying from 12% to 18%) in the foaming solution controls the membrane fraction and influences on structural characterization. For all samples, the ratio $(x_{fc}^{sq} + x_p^{sq}) / (x_{fc}^{hex} + x_p^{hex})$ is close to 1/3, which is consistent with previous works [36, 37]. Details in properties of membrane

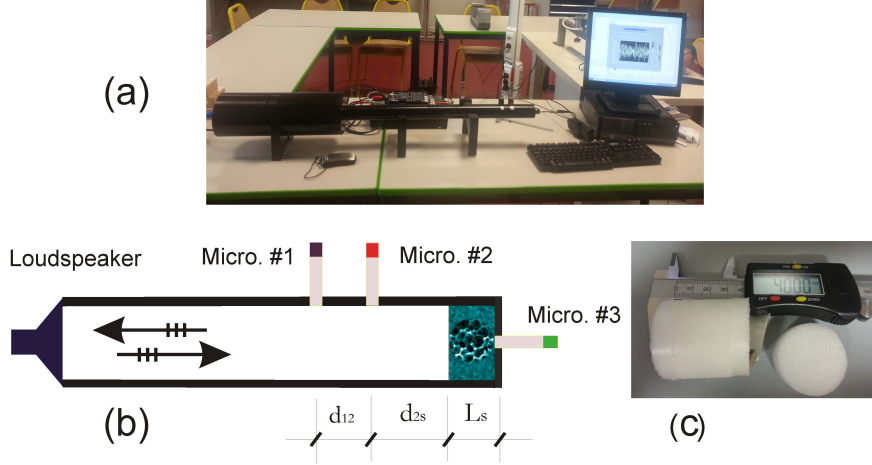


FIG. 3. (Color online) Three-microphone impedance tube measurement: experimental set-up (a), tube macroscopic configuration (b), and the foam sample (c).

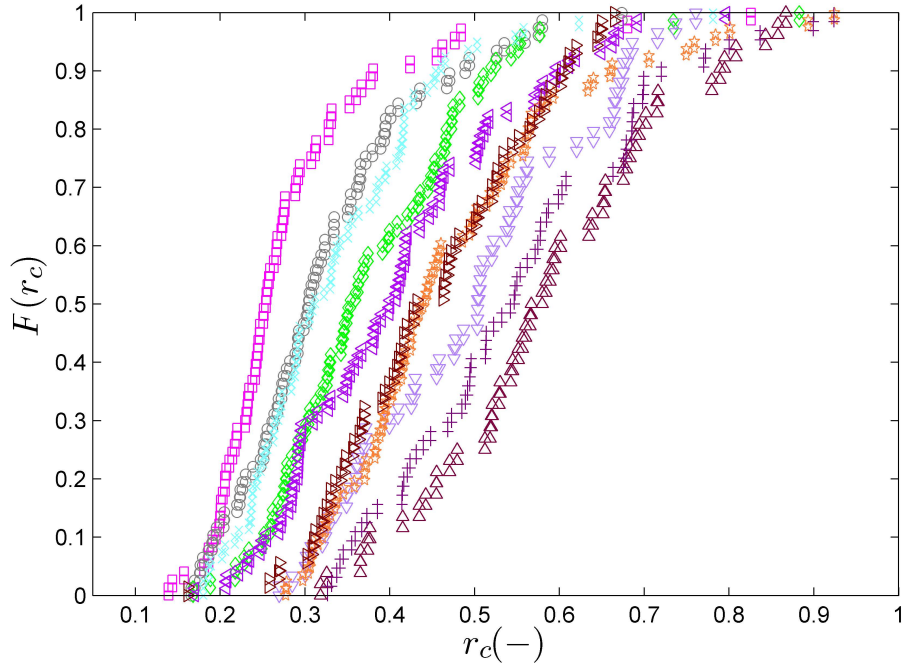


FIG. 4. (Color online) Distribution function of membrane closure rate measured on foam samples (D20 (\square), D14 (\circ), D1(\diamond), D2(\times), B9(∇), B16(\triangleleft), B5(\star), B4(\triangleright), B2(\triangle), and B1($+$)).

morphology, the closure rate of membrane in the larger windows r_c^{hex} tends to be slightly smaller than that in small ones r_c^{sq} for all sample foams. Consequently, this allows to consider the PUCs has an identical closure rate $r_c = (r_c^{sq} x_p^{sq} + r_c^{hex} x_p^{hex}) / (x_p^{sq} + x_p^{hex})$ instead of the identical membrane size mentioned in [27]. In addition, the measured morphological properties shown in Fig. 5 are very close with these provided in Refs [51, 52] for foams with

TABLE I. Static airflow resistivity and microstructural parameters measured on samples

Foam	C_{gel} (%)	x_p^{sq} (%)	x_{fc}^{sq} (%)	x_p^{hex} (%)	x_{fc}^{hex} (%)	r_c (-)	N_{fc}^{sq} (-)	N_{fc}^{hex} (-)	f_c (%)
D20	12	20.8	4.2	72.1	2.6	0.280	1	0	33.1
D14	13	18.4	8.1	64.9	8.6	0.323	2	1	43.6
D1	16	15.0	12.4	64.0	8.6	0.334	3	1	47.4
D2	16	12.7	16.1	56.6	14.6	0.397	3	2	57.0
B9	16	10.4	19.8	49.2	20.6	0.409	4	2	64.8
B16	17	8.2	23.6	45.5	22.7	0.495	4	3	72.9
B5	18	6.6	22.1	42.6	28.7	0.473	5	3	74.1
B4	18	6.1	17.9	26.1	50.9	0.448	4	5	83.2
B2	18	6.3	18.2	15.8	59.7	0.584	4	6	90.8
B1	18	3.4	24.9	11.2	61.3	0.551	5	7	94.2

monodisperse or relaxed structure.

As shown in Fig. 4, it is worth noting that the level of closure rate r_c increases upon to the rising of proportion of fully closed windows x_{fc} , this leads to an increase of membrane content from foam D20 to foam B1 (as shown in the last column in Table I. Based the open cell unit shown before and these morphological information, several type of PUC are reconstructed (see Fig. 4). It can be seen that each PUC has different set of parameters: N_{fc}^{sq} , N_p^{sq} , N_{fc}^{hex} , N_p^{hex} and the closed rate r_c . It should be noted that airflow resistivity corresponding to samples are characterized value obtained from the imaginary part of the low frequency behavior of the effective density as expression [38, 39] (see Eq. (D.5) in Appendix D). The effective density is assumed from the previous three-microphone impedance tube. The measured results of static resistivity show a significant increase upon the corresponding foam samples owning the membrane level of f_c from 30% to 90% (see permeability results shown Fig. 6 and Table S.VI in Supplemental Materials). This trend is very consistent with experimental data [20, 21, 28] and semi-empirical result provided by works from Doutres et al. [19, 40] (see also in Eq. (C.4) in Appendix C).

In terms of numerical results of non-acoustic properties, the configuration of each unit cell is considered based on its distribution of the fully closed faces (see also Supplemental Material). Of course, this distribution has no influence on the thermal characteristic length Λ' and the porosity ϕ . Other parameters are computed based on an averaging conductivity as follows. As in reconstruction of the representative cell, the PUC involves N_{fc}^{sq} of fully closed squares and N_{fc}^{hex} of fully closed hexagons. It could be easy to define the number of

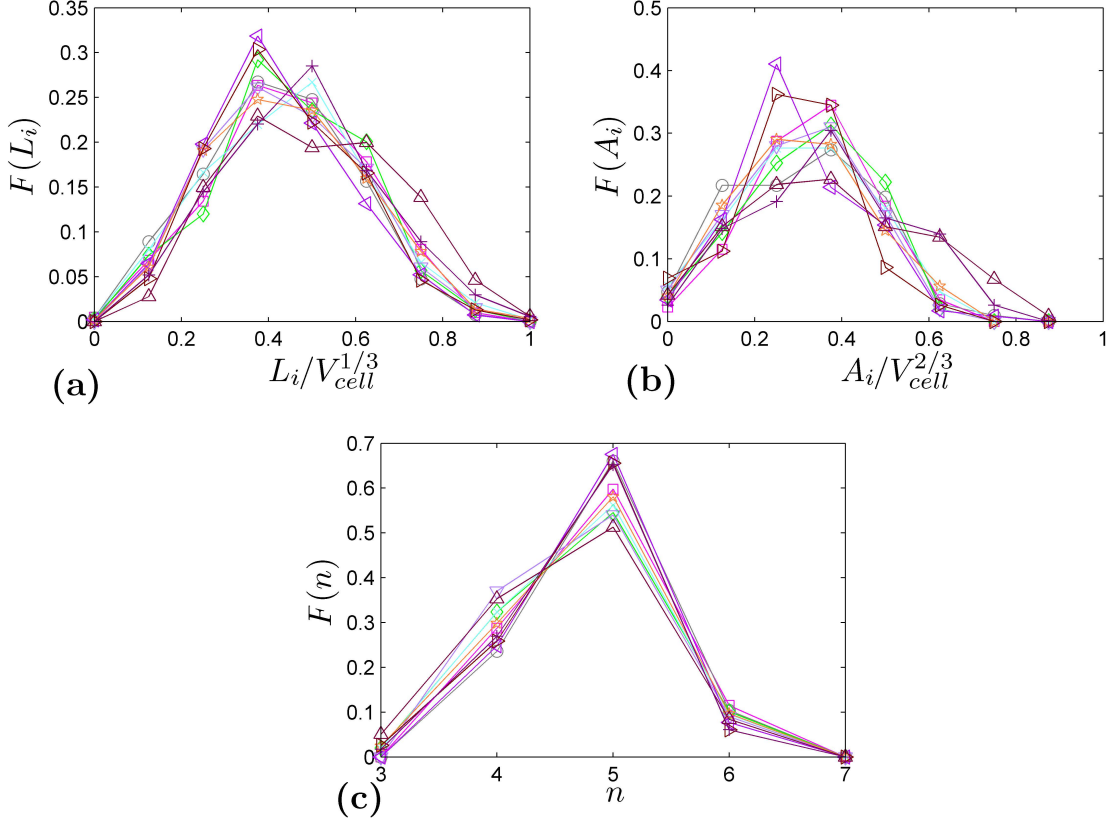


FIG. 5. (Color online) Morphological properties measured on foam samples (D20 (\square), D14 (\circ), D1(\diamond), D2(\times), B9(∇), B16(\triangleleft), B5(\star), B4(\triangleright), B2(\triangle), and B1($+$)): normalized edge length distributions(a), normalized face area distributions (b), and distributions of faces with n edges (c). Note that V_{cell} is the unit cell volume of $D_b^3/2$.

possible configurations n_{cf} as the following expression:

$$n_{cf} = \binom{6}{N_{fc}^{sq}} \times \binom{8}{N_{fc}^{hex}} \quad (5)$$

It is noted that the unit cell is not fully symmetry, so the averaging macroscopic transport property of each configuration $\bar{\tau}^i$ over all the directions is calculated as [49],

$$\bar{\tau}^i = \frac{1}{3} \text{tr}(\boldsymbol{\tau}^i) \quad (6)$$

In which, the τ_{xx}^i , τ_{yy}^i , τ_{zz}^i are three components of conductivity $\boldsymbol{\tau}^i$ along the x , y and z direction, respectively. Noted that n_{cf} is total possible configurations of the PUC, so

$\tau_{xx}^i \equiv \tau_{yy}^i \equiv \tau_{zz}^i$, with $\tau_{kk}^i = \{\tau_{kk}^i \mid i = 1, 2, \dots, n_{cf}\}$ and $kk = xx, yy, zz$. In addition, we are able to define the conductivity along y and z direction of a configuration from that along x direction of other configurations (Detail about defining these configurations, see Supplemental Material).

Then, the averaging macroscopic conductivity is deduced by,

$$\bar{\tau} = \frac{1}{n_{cf}} \sum_{i=1}^{n_{cf}} \bar{\tau}^i = \frac{1}{n_{cf}} \sum_{i=1}^{n_{cf}} \tau_{kk}^i \quad (7)$$

As shown in Fig. 6, the computed and the characterized non-dimensional macroscopic parameters are in good agreement in term of their dependence on the membrane fraction f_c . In general, the membrane content has a significant effect on all macroscopic transport properties, and these influences are in good agreement with numerical results [27] and imperial equations [19], note that our parameter f_c has a directly link with both the membrane closure rate and the reticulated rate in these reference works (see Sec. IV B. Following an increase of f_c , two characteristic lengths (Λ' , Λ) and viscous permeability k_0 decrease sharply, while high frequency tortuosity α_∞ shows a significant increase. This leads to an interesting sound absorption performance of membrane foam layer indicated in the following section.

B. Acoustic property

In terms of sound absorption ability, as illustrated in Fig. 7, the results show that this class of foam samples has distinct behaviors in term of sound performance for given frequency range, also our simulated results are in agreement with experimental data and characterized results. Generally, it is clearly that the membrane fraction of foams has strongly influence on their sound absorption performance in different frequency bands in the range from 4 to 4500 Hz. The samples owning the lowest (foam D20) and highest (foams B2 ($\alpha \approx 0.2$) and B1 ($\alpha \approx 0.15$)) membrane fraction show a poor sound absorbing capacity ($\alpha \leq 0.5$) in whole range of frequency (for the sample B1, see Fig. S.9 in Supplemental Material). It means that in this scale of cell size, a layer made of opened-cell or closed-cell foams is not good for the sound absorption applications. Of course it is here not mentioned the case that its absorbing coefficient is improved by increase in its thickness. Interestingly, with the middle level of membrane content, the absorption property is significantly improved.

In the trend of increasing of f_c (sample D1, D2, and B9), as mentioned previously, the enhanced low frequency sound absorption correlates with an increase in tortuosity with a decrease of the other transport parameters. For samples (B16, B4 and B5), however, this enhanced of mean value of SAC is accompanied with a decrease of the peak of SAC in the whole frequency range. Fig. 8 illustrates of a sound absorbing chart depended on frequency together membrane levels, it is seen that the computational chart (the left part) is very close with the experimental one (the right part). These charts figured out clearly that the range of membrane level produces a high sound absorption ability in a large frequency range of interested. In addition, the charts also demonstrate the moving of location of frequency with a SAC peak and the high SAC in the low frequency range of high membrane foams.

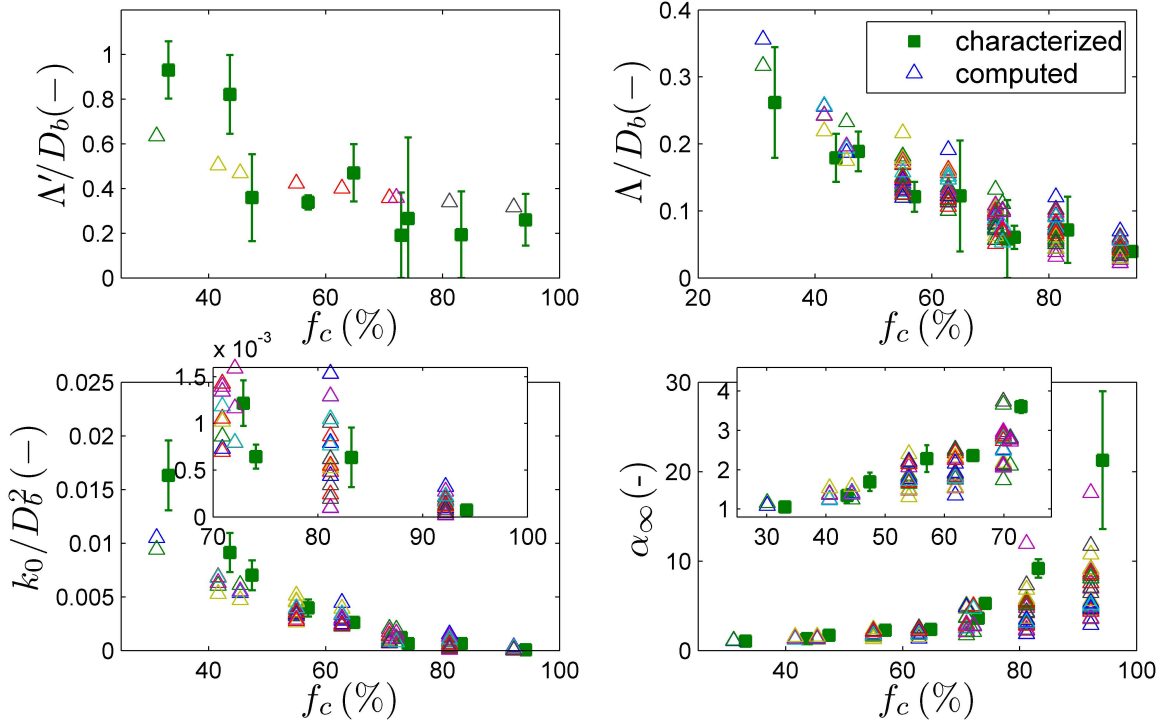


FIG. 6. (Color online) Dependence of characterized(\square) and computed (\triangle) dimensionless transport properties on the membrane fraction.

Our predictions are also compared with measurements and models available in the literature. The indirect method as proposed by Panneton and Only [38, 39] provides an experimental characterization of the macroscopic parameters (Λ , α_∞ , Λ and k'_0) from measured effective density and bulk modulus (assuming a 3-microphones impedance tube, and available estimates of σ and ϕ) by using analytical solutions derived from the JCAL model (see

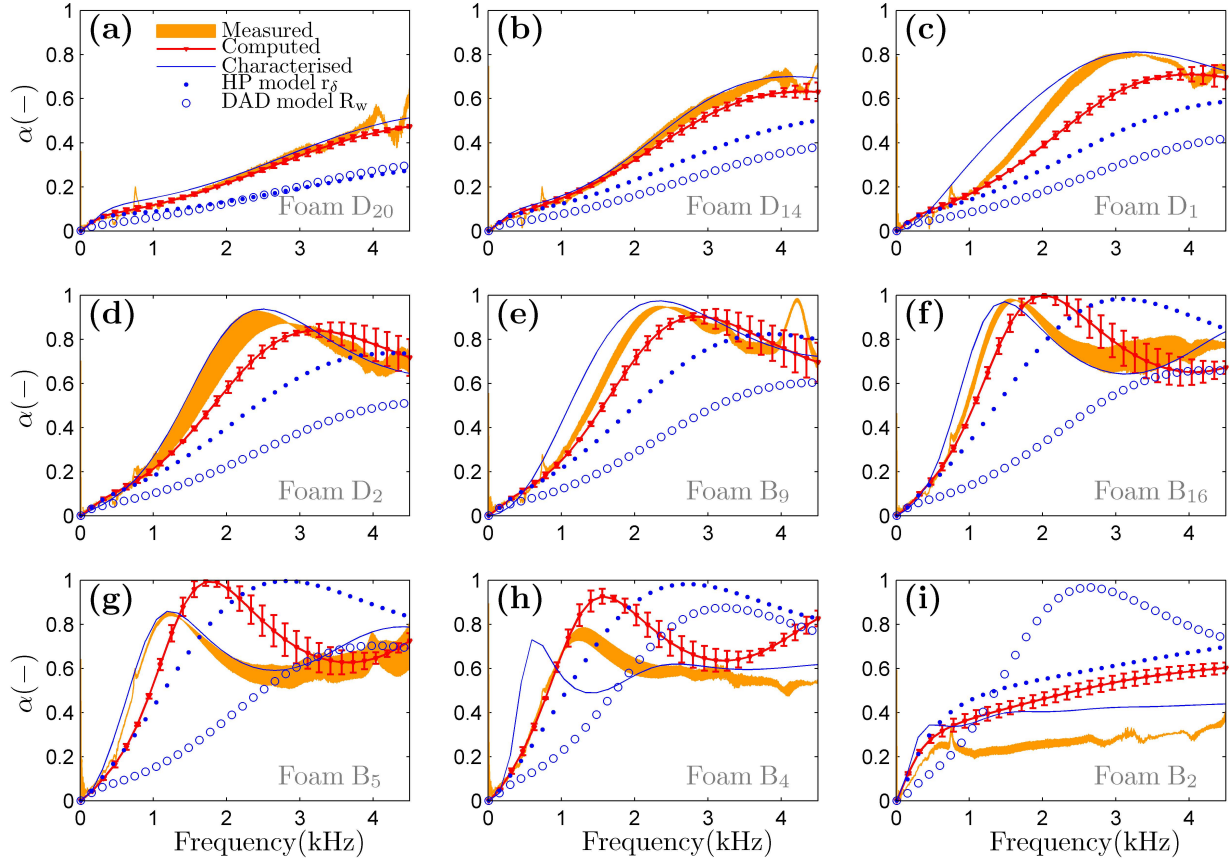


FIG. 7. (Color online) Sound absorption coefficients (SAC) of samples: experiments (filled zone), computations (thick continuous lines), characterizations (thin continuous lines), HP method (point markers), and DAD method (circle markers).

Appendix B). A simplified approach, referred to as a semi-empirical (2-parameter) model, has been proposed by Doutres et al. [19] in assuming a micro-/macro correlation based on the cell size D_b and a reticulation rate $R_w = x_p$, (see Appendix C). The third model is a numerical approach having the same procedure with our work but the different reconstructed PUCs including a membrane rate r_δ . This provided by Hoang and Perrot [27, 28], this work uses a PUC having membrane of equal size formed in all windows. This size increases from 0 (for open structure), then continuously increase to fully close squares and finally to cover the hexagons (closed cell structure). For a given porosity and cell size, following an increase of membrane size, the numerical computations are performed to investigate the varying of permeability. The PUC, having a membrane size that produces a similar numerical permeability in comparison with experimental or characterized data, is selected to represent foam material. (see Table S.V-VI in Supplemental Material for a detailed view about calculated

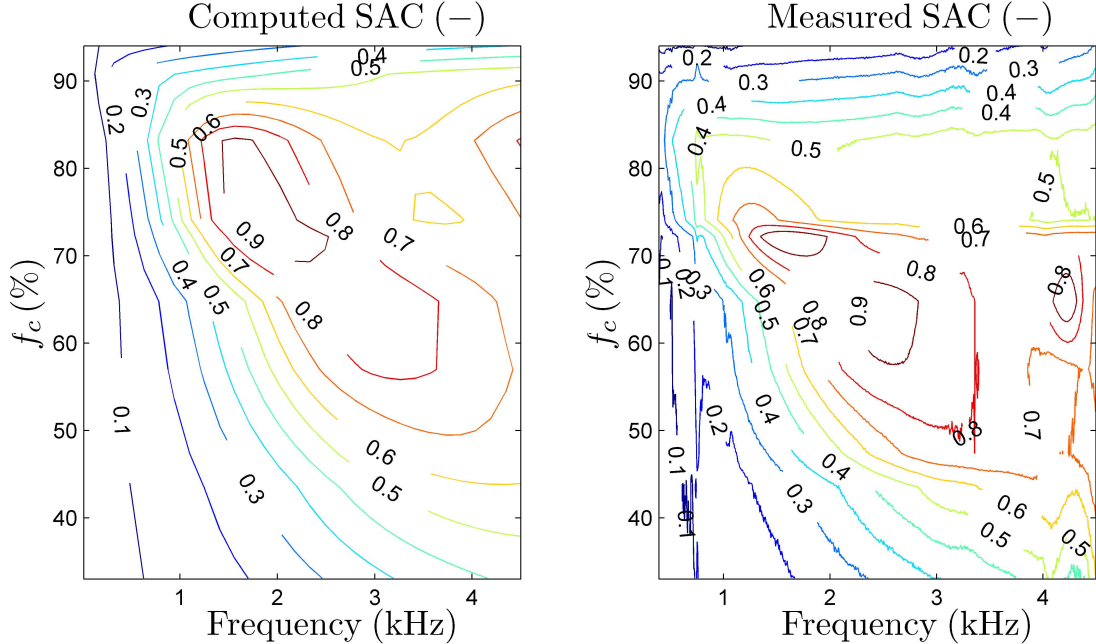


FIG. 8. (Color online) Illustration of SAC: computations (left panel) and measurements (right panel).

transport parameters of the literature model of r_δ .

Fig. 7 shows that Doutres et al. (DAD) model (semi-empirical method) as well as Hoang and Perrot (HP) model (numerical method with equivalent membrane closure rate) fail to predict sound absorbing behavior of such foams which have both partially and fully closed windows. Note that these original models shown very good predictions of SAC in their studied materials with mostly partially closed windows (see SEM image of materials, Figure 1 in Refs. [27, 28] and Figure 8 in Ref. [20]), or fully closed windows and opened windows (see Figure 1 in Ref. [40]). How to use these models to characterize membrane foams? A detailed discussion on this statement will be described in the forthcoming part.

C. Comment on models of acoustic membrane foams

In a view point of modeling acoustical membrane foams, some interesting comments can be made based on the predicting ability of transport properties and SAC of the proposed as well as comparative models. Because of neglecting fully closed windows [20, 27, 28] or partially closed windows [19, 40], two existing models do not capture the wave propagation phenomena in advanced morphology of real foams composing of both fully and partially faces

(with very poor prediction of the sound absorbing behavior, see Fig. 7). The presented model allows for accounting such materials and handles the limitations of previous models. We suggest that (i) the periodic unit cell for finite element simulation should involve a number of fully closed faces, and (ii) the semi-empirical approach with reticulated rate R_w or cell openness p should also including a fraction of partially closed faces (x_p) and corresponding their closure rate of membrane (r_c). Of course, by adding a number of fully closed faces in PUC used to numerical simulations, our computed results show a very good prediction in compared with results based HP estimates (see the points in Fig. 7) and Park's work (see Figure 6.(a) in Ref. [41]). This is clearly confirmed for the first suggestion, and also for the second one as follows.

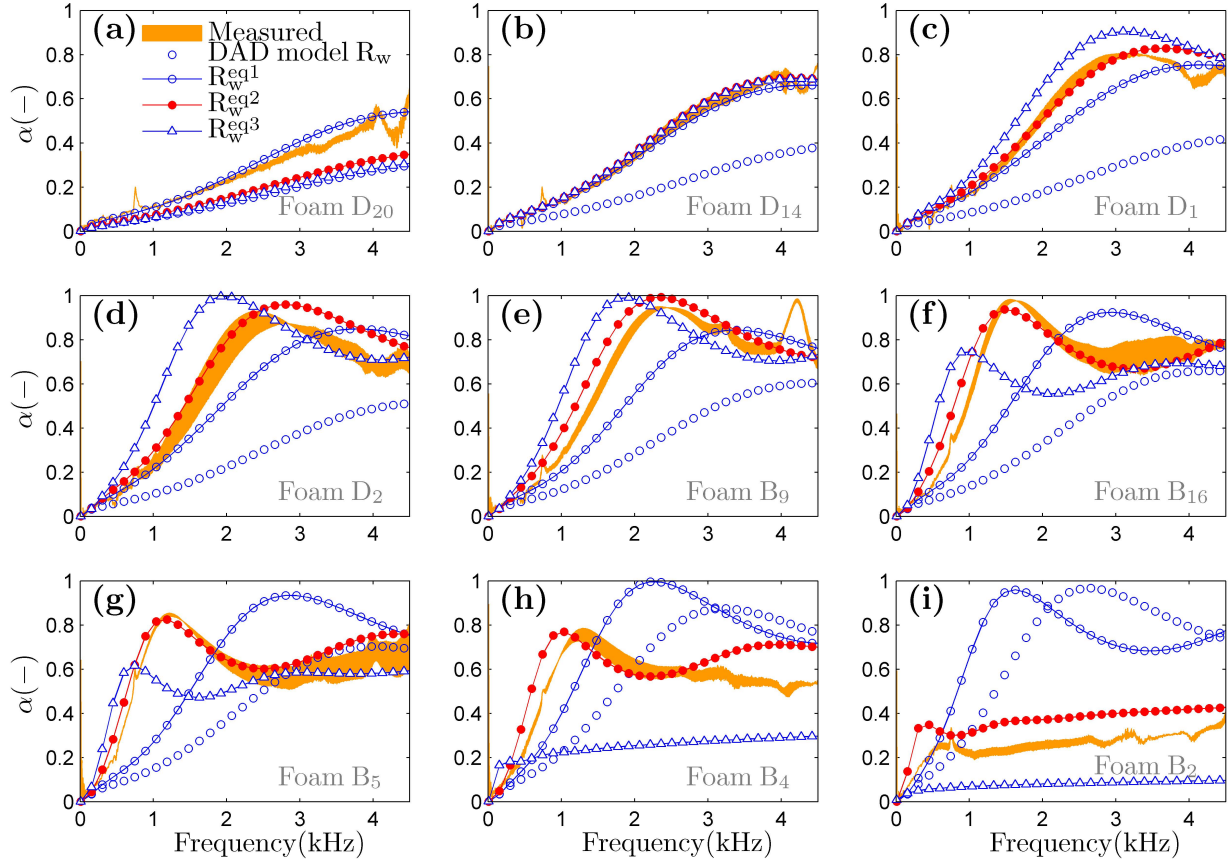


FIG. 9. (Color online) Sound absorption coefficients defined from the developed semi-empirical model with an equivalent reticulated rate: experiments (filled zone), computations (thick continuous lines), original DAD method (circle markers), developed DAD model (solid lines with markers: R_w^{eq1} (circles), R_w^{eq2} (filled circles), R_w^{eq3} (filled triangles)).

In the next, we develop the DAD semi-empirical estimates based on an equivalent retic-

ulated rate R_w^{eq} that characterized by different ways. The first equivalent reticulated rate is defined directly based on the morphology characterizations of local geometry of materials as,

$$R_w^{eq1} = x_p - r_c x_p \quad (8)$$

The second equivalent reticulated rate is estimated by an equivalent macroscopic transport property for the case of airflow resistivity. It means that Eq. (C.4) in Appendix C is used to find this equivalent ratio,

$$R_w^{eq2} = \left(\frac{\sigma^{open}}{\sigma} \right)^{1/1.1166} \quad (9)$$

Similarly, considering a semi-empirical model with an equivalent high frequency tortuosity, the third equivalent reticulated rate is defined by,

$$R_w^{eq3} = \left(\frac{\alpha_\infty^{open}}{\alpha_\infty} \right)^{1/0.3802} \quad (10)$$

in which, $\sigma^{open} = 1674 \text{ Nms}^{-4}$ and $\alpha_\infty^{open} = 1.05$ and are airflow resistivity and high frequency tortuosity obtained from our computations for open cell structure foams (with cell size of D_b and porosity ϕ), respectively, resistivity; σ and tortuosity α_∞ are characteristic values (Table S XX Supplemental Material). These results are very consistent with the given value $\alpha_\infty^{open} = 1.05$ in Eq. (C.3) and the analytical result $\sigma^{open} = C^\beta (C_r^\rho r / L^2)^2 = 1781 \text{ Nms}^{-4}$ in Eq. (C.4)

As shown in Fig. 9, it is seen clearly that all prediction curves of SAC behavior (lines with markers) has a fitting improvement by three equivalent rates in comparison with that from the original rate of proportion of open windows (circle markers). Here, we just employ new equivalent reticulated rate, and all of equations in the semi-empirical model has no modifying as shown in Appendix C. In particular, semi-empirical model with the reticulated rate R_w^{eq1} shows a good SAC predictions only for two samples D20 and D14 with a lower membrane levels (see the thin lines with circular marker in Fig. 8(a-b)), and the model of R_w^{eq3} shows a quite good predictions of SAC for samples named D14, D1, D2 and B9 (see Fig. 9(b-e), the continuous lines with filled triangular marker). In contrary, for the rate R_w^{eq2} deduced from equivalent of resistivity, it is seen that this method can accurately model the sound absorption behavior of the closed cell foam materials in whole range of membrane

level (see Fig. 9(b-i)). Interestingly, the comparison between two SAC results obtained from characterized work (the thin continuous line in Fig. 7) and semi-empirical model of equivalent rate R_w^{eq2} (the continuous line with filled circular marker in Fig. 9) shows a very good agreement. It can be concluded that the empirical model developed based on equivalent tortuosity α_∞ or resistivity σ can predict accurately the sound absorption capability. The transport properties of all semi-empirical models are listed in Table S.VII in Supplemental Material.

Let us back with the above the HP numerical model. Even though it is also proposed based on the equivalent viscous permeability, this model fails to simulate the SAC of studied materials (for both cases identical membrane size (r_δ) and identical membrane closure rate (r_δ^1), see Fig .S.8 in Supplemental Material). Our model can capture sound absorbing properties, although our numerical and experimental permeability have a slightly difference. This means that the task of reconstruction of PUC plays a significant role in the numerically simulations of such membrane foam materials, because this requires a capturing the influence of not only permeability but also other macroscopic transport properties of materials.

V. CONCLUSION

A three-dimensional idealized periodic unit cell (PUC)-based method to obtain the acoustic properties of high porous foam samples was described in this work. The PUC based on regular truncated octahedron packing is used for this hybrid multi-scale modeling. In this approach, first, some laboratory measurements of porosity and image processing techniques are taken. Different unit cells are then reconstructed from bubble size and membrane morphology characterization to compute macroscopic parameters from numerical homogenization. These later values serve in a sense as bridges between microstructure and acoustical macro-behavior with microphysical and micromechanical foundations. The numerical results are generally in good agreement with experimental values obtained from the measurements of standing wave tube.

As illustration of the obtained sound absorbing chart, it can be seen clearly that for a certain foam within given porosity and pore size, we are able to control their membrane morphology to archive the target sound absorption capacity in the frequency range of interest. For 20-mm thick layer made from membrane cellular foams with cell size 0.8 mm and

porosity of 0.98, to reach the high absorption quality, the membrane level is should be kept in the range of 45 to 85% by using the gelatin concentration C_{gel} around 16%. In this target range of membrane fraction, it can be noted that the foam absorber can archive the high SAC in the high frequency band with f_c around value of lower bound of 80%, and the low frequency band with f_c round the value of upper bound of 50%. The context of foaming morphology in our proposed approach can be adopted for other purpose in mechanical investigation of such foam-based materials. The development of an advanced modeling of the membrane content as well as few comments for literature models, such as the one proposed in this communication.

ACKNOWLEDGMENTS

This work was part of a project supported by ANRT (Grant no. ANR-13-RMNP-0003-01). The work of V. H. Trinh was supported by a fellowship awarded by the Government of Vietnam (Project 911).

APPENDIX

Appendix A: Reconstruction of periodic unit cell

In this appendix, we reconstruct the periodic unit cell based on Kelvin pattern. A part of the 1/96 periodic unit cell is approximated as 1/4 triangular tube and 1/8 octahedron placed at their junction of node (see Fig. 10). It is easy to find the coordinates of 7 vertices of this skeleton listed as follows: A(0, $r/2\tan\beta$, 0); B($r/2$, 0, 0); C(0, $-r/2\tan\beta$, 0); F($r/2$, 0, $-r/2$); J($r/2 + L_l\sqrt{2}/4$, $-L_l\sqrt{2}/4$, 0); K($L_l\sqrt{2}/4$, $-L_s\sqrt{2}/4$, 0) and M($r/2 + L_l\sqrt{2}/4$, $-L_l\sqrt{2}/4$, $-r/2$). In which, $L_l = (D_b/4 - r/2)\sqrt{2}$, $L_s = [D_b/4 - r/2(\sqrt{6} - 1)]\sqrt{2}$, $\beta = 3\pi/4 - \alpha$ with $\tan\alpha = \sqrt{3}/(\sqrt{3} - \sqrt{2})$.

The total solid volume of unit cell is the volume of 12 nodes and 24 ligaments (12 edges on hexagonal faces and 24 edges shared with the neighboring cells), given by

$$V_s = 96 \times (V_{ABFJKM} + V_{ABCF}) = 6\sqrt{3}Lr^2 + (4\tan\beta - 6 - \sqrt{6})r^3 \quad (\text{A.1})$$

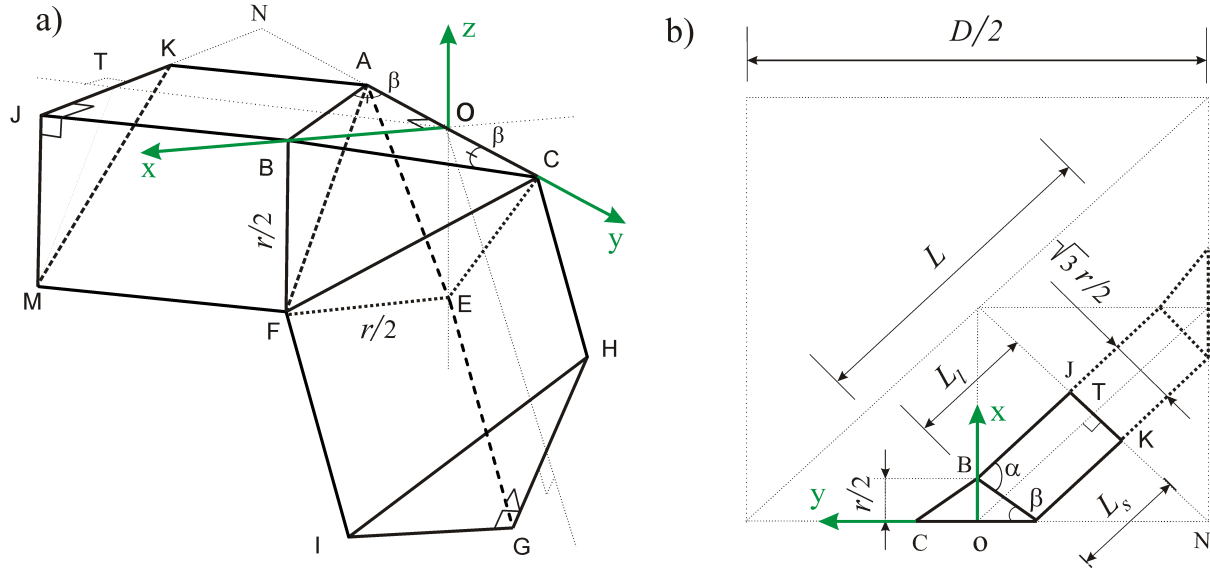


FIG. 10. (a) Detail of the coordinates of the basic vertex in a $1/48$ open unit cell having ligaments of equilateral triangular cross section of edge size r . (b) Diagram shows the relations between the angular and length parameters of node and ligament (top view of the skeleton).

The porosity of the open cell structure can be defined as,

$$\phi = 1 - \frac{3\sqrt{6}}{16} \left(\frac{r}{L}\right)^2 - \frac{4\tan\beta - 6 - \sqrt{6}}{16\sqrt{2}} \left(\frac{r}{L}\right)^3 \quad (\text{A.2})$$

Solving Eq. (A.2), it is obtained the ligament size r/L as a function of porosity ϕ ,

$$\frac{r}{L} = \frac{P_2}{3P_3} \left[1 - \cos \frac{\arccos(\chi) - 2\pi}{3} \right] \quad (\text{A.3})$$

where $\chi = \frac{P_2^3 - 27P_3P_0}{2\sqrt{P_2^3}}$, with $P_0 = 1 - \phi$, $P_2 = \frac{3\sqrt{6}}{16}$, and $P_3 = \frac{4\tan\beta - 6 - \sqrt{6}}{16\sqrt{2}}$. Hence, one obtain an approximate expression from Eq. (A.3) as $r/L = 0.5833(1 - \phi)^{0.521}$.

Appendix B: Numerical estimations of transport property

Two purely geometrical parameters (ϕ , Λ') are defined directly from the local geometry via an unit cell Ω (of Ω_f fluid-filled domain and $\partial\Omega$ fluid-solid interface) as,

$$\phi = \frac{\int_{\Omega_f} dV}{\int_{\Omega} dV}, \quad \Lambda' = 2 \frac{\int_{\Omega} dV}{\int_{\partial\Omega} dS} \quad (\text{B.1})$$

The remaining transport property is computed from the numerical solutions of three group of governing equations into the unit cell. Firstly, the low Reynolds number flow of an incompressible Newtonian fluid is governed by the usual Stokes equations in the fluid phase Ω_f ,[\[42\]](#):

$$\eta \Delta \mathbf{v} - \nabla p = -G \text{ with } \nabla \cdot \mathbf{v} = 0 \text{ in } \Omega_f \quad (\text{B.2a})$$

$$\mathbf{v} = 0 \text{ on } \partial\Omega \quad (\text{B.2b})$$

$$\mathbf{v} \text{ and } p \text{ are } \Omega - \text{periodic} \quad (\text{B.2c})$$

where $G = \nabla p^m$ is the macroscopic pressure gradient acting as a source term. Symbols \mathbf{v} and p are the velocity and pressure of the fluid respectively. In general, \mathbf{v} satisfies the non-slip condition ($\mathbf{v}=0$) at $\partial\Omega$. It can be shown that the local field of the static viscous permeability are obtained from the local velocity field as,

$$\mathbf{k}_0 = -\frac{\eta}{G} \mathbf{v} \quad (\text{B.3})$$

The static viscous permeability k_0 and static viscous tortosity α_0 are calculated by the standard definitions below,

$$k_0 = \phi \langle \mathbf{k}_0 \rangle, \quad \alpha_0 = \frac{\langle \mathbf{k}_0^2 \rangle}{\langle \mathbf{k}_0 \rangle^2} \quad (\text{B.4})$$

The symbol $\langle \cdot \rangle$ denotes a fluid-phase averaging operator, $\langle \cdot \rangle = \int_{\Omega_f} (\cdot) dV$.

Secondly, at the high frequency range with ω large enough, the viscous boundary layer becomes negligible and the fluid tends to behave as a perfect one, having no viscosity except in a boundary layer. Consequently, the perfect incompressible fluid formally behaves according to the electrical conduction problem [\[2, 45, 46\]](#):

$$\nabla \cdot \mathbf{E} = 0 \text{ with } \mathbf{E} = -\nabla \varphi + \mathbf{e}, \text{ in } \Omega_f \quad (\text{B.5a})$$

$$\mathbf{E} \cdot \mathbf{n} = 0, \text{ in } \partial\Omega_f \quad (\text{B.5b})$$

$$\varphi \text{ is } \Omega - \text{periodic} \quad (\text{B.5c})$$

where \mathbf{e} is a given macroscopic electric field, \mathbf{E} the solution of the boundary problem having $-\nabla \varphi$ as a fluctuating part, and \mathbf{n} is unit normal to the boundary of the pore region.

The high frequency tortuosity α_∞ and the viscous characteristic length Λ are calculated:

$$\alpha_\infty = \langle \mathbf{E} \cdot \mathbf{e} \rangle, \quad \Lambda = \frac{\langle \mathbf{E}^2 \rangle}{\langle \mathbf{E} \rangle^2} \quad (\text{B.6})$$

Now, all transport parameters of reference model are available.

Appendix C: Semi-empirical estimations of transport property

This estimation is provided from reference model by Doutres et al.[19, 40] for membrane cellular foams. In this model, a simplified micro-/macro link is presented based on a cell size D_b and a reticulated rate R_w . This work uses the classical JCA model to predict the sound absorption efficiency, this model is known as the 5-parameters (ϕ , Λ' , Λ , σ , and α_∞). Firstly, the porosity and the thermal characteristic length of materials is calculated as,

$$\phi = \frac{C_p}{B^2}, \quad \Lambda' = D_b \frac{8 [1 - (2\sqrt{3} - \pi)/B^2\sqrt{2}] / 3A}{1 + 2\sqrt{3} - R_w(1 + 2\sqrt{3} - 4\pi/B\sqrt{3})} \quad (\text{C.1})$$

where $C_p = (2\sqrt{3} - \pi)/\sqrt{2}$, $A = D_b/\sqrt{2}$ and $B = D/(Ar\sqrt{2})$.

Then, the viscous characteristic length is defined as a function of the reticulated rate R_w ,

$$\Lambda' / \Lambda = 1.55 / R_w^{0.6763} \quad (\text{C.2})$$

The high frequency tortuosity is defined as,

$$\alpha_\infty = 1.05 / R_w^{0.6763} \quad (\text{C.3})$$

Finally, the airflow resistivity is deduced by,

$$\sigma = C^\beta (C_r^\rho r / L^2)^2 / R_w^{1.1166} \quad (\text{C.4})$$

in which $C^\beta = 128\alpha_\infty\eta/c_g^2$ and $C_r^\rho = 3\pi/8\sqrt{2}$.

Appendix D: Characterized estimations of transport and effective property

The characterization method [38, 39] is presented for determining the normal incidence sound absorption coefficient and the effective properties of tested materials based on the experimental data with two measured pressure transfer functions H_{12} and H_{23} . The complex reflection coefficient of sample is deduced:

$$R = \frac{\exp(jd_{12}k_0) - H_{12}}{H_{12} - \exp(-jd_{12}k_0)} \exp(2jk_0L_s) \quad (\text{D.1})$$

where d_{12} is the distance between microphone 1 and 2 (see Fig. 3), k_0 denotes the wave number in the ambient fluid.

The pressure ratio H_0 between the front and the rear of the sample is estimated as,

$$H_0 = \frac{1 + R}{\exp(jk_0L_s) - R/\exp(jk_0L_s)} H_{23} \quad (\text{D.2})$$

Then, the wave number $k_c(\omega)$ and the characteristic impedance $Z_c(\omega)$ are given by,

$$k_c(\omega) = \frac{1}{L_s \cos(H_0)}, \quad Z_c(\omega) = jZ_s \cot(k_c(\omega)L_s), \quad \text{with } Z_s/Z_0 = \frac{1 + R}{1 - R} \quad (\text{D.3})$$

The effective density and the effective bulk modulus properties of materials are also evaluated as,

$$\rho(\omega) = Z_c(\omega)k_c(\omega)/\omega, \quad K(\omega) = Z_c(\omega)\omega/k_c(\omega) \quad (\text{D.4})$$

Finally, five macroscopic properties of materials are determined from the measured effective density $\rho(\omega)$ and bulk modulus $K(\omega)$ using the indirect method proposed by Panneton and Olny[38, 39] as follows,

$$\sigma = \lim_{\omega \rightarrow 0} [\Im(\omega\rho)] \quad (\text{D.5})$$

$$\alpha_\infty = \frac{\phi}{\rho_0} \left[\Re(\rho) - \sqrt{\Im(\rho)^2 - \left(\frac{\sigma\phi}{\omega}\right)^2} \right] \quad (\text{D.6})$$

$$\Lambda = \frac{\alpha_\infty}{\phi} \sqrt{\frac{2\rho_0\eta}{\omega\Im(\rho)(\rho_0\alpha_\infty/\phi - \Re(\rho))}} \quad (\text{D.7})$$

$$\Lambda' = 2 \sqrt{\frac{\eta}{P_r \rho_0 \omega} \left\{ -\Im \left(\left[\frac{1 - K/K_a}{1 - \gamma K/K_a} \right]^2 \right) \right\}} \quad (\text{D.8})$$

$$k'_0 = \frac{\phi \eta}{P_r \rho_0 \omega} \left\{ -\Re \left(\left[\frac{1 - K/K_a}{1 - \gamma K/K_a} \right]^2 \right) \right\}^{-1/2} \quad (\text{D.9})$$

in which K_a denotes adiabatic bulk modulus.

-
- [1] S. Gasser, F. Paun, and Y. Bréchet, “Absorptive properties of rigid porous media: Application to face centered cubic sphere packing,” *J. Acoust. Soc. Am.* **117**, 2090-2099 (2005).
 - [2] C. Perrot, F. Chevillotte, R. Panneton, J.-F. Allard, and D. Lafarge, “On the dynamic viscous permeability tensor symmetry,” *J. Acoust. Soc. Am.* **124**, EL210-EL217 (2008).
 - [3] F. Chevillotte, C. Perrot, and R. Panneton, “Microstructure based model for sound absorption predictions of perforated closed-cell metallic foams,” *J. Acoust. Soc. Am.* **128**, 1766-1776, (2010).
 - [4] R. Venegas and O. Umnova, “Acoustical properties of double porosity granular materials,” *J. Acoust. Soc. Am.* **130**, pp. 2765-2776, (2011).
 - [5] F. Chevillotte, C. Perrot, and E. Guillon, “A direct link between microstructure and acoustical macro-behavior of real double porosity foams,” *J. Acoust. Soc. Am.* **134**, pp. 4681-4690, (2013).
 - [6] L. J. Gibson and M. F. Ashby, *Cellular solids: structure and properties*: Cambridge university press, 1999.
 - [7] C. Perrot, R. Panneton, and X. Olny, “Periodic unit cell reconstruction of porous media: Application to open-cell aluminum foams,” *J. Appl. Phys.* **101**, p. 113538, (2007).
 - [8] N. Kino and T. Ueno, “Evaluation of acoustical and non-acoustical properties of sound absorbing materials made of polyester fibres of various cross-sectional shapes,” *Appl. Acoust.* **69**, pp. 575-582, (2008).
 - [9] L. Boeckx, M. Brennan, K. Verniers, and J. Vandebroek, “A numerical scheme for investigating the influence of the three dimensional geometrical features of porous polymeric foam on its sound absorbing behavior,” *Acta Acust. United Ac.* **96**, pp. 239-246, (2010).

- [10] O. Doutres and N. Atalla, “A semi-empirical model to predict the acoustic behaviour of fully and partially reticulated polyurethane foams based on microstructure properties,” in *Acoustics 2012*, (2012).
- [11] D. L. Johnson, J. Koplik, and R. Dashen, “Theory of dynamic permeability and tortuosity in fluid-saturated porous media,” *J. Fluid Mech.* **176**, pp. 379-402, (1987).
- [12] Y. Champoux and J. F. Allard, “Dynamic tortuosity and bulk modulus in airsaturated porous media,” *J. Appl. Phys.* **70**, pp. 1975-1979, (1991).
- [13] D. Lafarge, P. Lemarinier, J. F. Allard, and V. Tarnow, “Dynamic compressibility of air in porous structures at audible frequencies,” *J. Acoust. Soc. Am.* **102**, pp. 1995-2006, (1997).
- [14] C.-Y. Lee, M. J. Leamy, and J. H. Nadler, “Acoustic absorption calculation in irreducible porous media: A unified computational approach,” *J. Acoust. Soc. Am.* **126**, pp. 1862-1870, (2009).
- [15] X. Cai, J. Yang, and G. Hu, “Optimization on microlattice materials for sound absorption by an integrated transfer matrix method,” *J. Acoust. Soc. Am.* **137**, pp. EL334-EL339, (2015).
- [16] E. Lind-Nordgren and P. Gransson, “Optimising open porous foam for acoustical and vibrational performance,” *J. Sound Vib.* **329**, pp. 753-767, (2010).
- [17] X. Wang and T. J. Lu, “Optimized acoustic properties of cellular solids,” *J. Acoust. Soc. Am.* **106**, pp. 756-765, (1999).
- [18] K. Gao, J. van Dommelen, and M. Geers, “Microstructure characterization and homogenization of acoustic polyurethane foams: Measurements and simulations,” *Int. J. Solids Struct.* **100**, pp. 536-546, (2016).
- [19] O. Doutres, N. Atalla, and K. Dong, “A semi-phenomenological model to predict the acoustic behavior of fully and partially reticulated polyurethane foams,” *J. Appl. Phys.* **113**, p. 054901, (2013).
- [20] C. Perrot, F. Chevillotte, M. T. Hoang, G. Bonnet, F.-X. Bécot, L. Gautron, et al., “Microstructure, transport, and acoustic properties of open-cell foam samples: Experiments and three-dimensional numerical simulations,” *J. Appl. Phys.* **111**, p. 014911, (2012).
- [21] N. Kino, G. Nakano, and Y. Suzuki, “Non-acoustical and acoustical properties of reticulated and partially reticulated polyurethane foams,” *Appl. Acoust.* **73**, pp. 95-108, (2012).
- [22] V. H. Trinh, M. T. Hoang, C. Perrot, V. Langlois, Y. Khidas, and O. Pitois, “A Systematic Link between Microstructure and Acoustic Properties of Foams: A Detailed Study on the

- Effect of Membranes,” in Poromechanics VI, ed, pp. 1405-1412 (2017).
- [23] O. Doutres, M. Ouisse, N. Atalla, and M. Ichchou, “Impact of the irregular microgeometry of polyurethane foam on the macroscopic acoustic behavior predicted by a unit-cell model,” *J. Acoust. Soc. Am.* **136**, pp. 1666-1681, (2014).
- [24] K. Yasunaga, R. Neff, X. Zhang, and C. Macosko, “Study of cell opening in flexible polyurethane foam,” *J. Cell. Plast.* **32**, pp. 427-448, (1996).
- [25] X. Zhang, H. Davis, and C. Macosko, “A new cell opening mechanism in flexible polyurethane foam,” *J. Cell. Plast.* **35**, pp. 458-476, (1999).
- [26] C. Zhang, J. Li, Z. Hu, F. Zhu, and Y. Huang, “Correlation between the acoustic and porous cell morphology of polyurethane foam: Effect of interconnected porosity,” *Mater. Des.* **41**, pp. 319-325, (2012).
- [27] M. T. Hoang and C. Perrot, “Solid films and transports in cellular foams,” *J. Appl. Phys.* **112**, p. 054911, (2012).
- [28] M. T. Hoang, G. Bonnet, H. T. Luu, and C. Perrot, “Linear elastic properties derivation from microstructures representative of transport parameters,” *J. Acoust. Soc. Am.* **135**, pp. 3172-3185, (2014).
- [29] J. Rubinstein and S. Torquato, “Diffusioncontrolled reactions: Mathematical formulation, variational principles, and rigorous bounds,” *J. Chem. Phys.* **88**, pp. 6372-6380, (1988).
- [30] D. L. Weaire and S. Hutzler, *The physics of foams*, (Oxford University Press, 2001).
- [31] I. Cantat, S. Cohen-Addad, F. Elias, F. Graner, R. Hhler, O. Pitois, et al., *Foams: structure and dynamics*, (Oxford University Press, 2013).
- [32] B. Haffner, Y. Khidas, and O. Pitois, “The drainage of foamy granular suspensions,” *J. Colloid Interf. Sci.* **458**, pp. 200-208, (2015).
- [33] M. R. Stinson and G. A. Daigle, “Electronic system for the measurement of flow resistance,” *J. Acoust. Soc. Am.* **83**, pp. 2422-2428, (1988).
- [34] T. Iwase, Y. Izumi, and R. Kawabata, “A new measuring method for sound propagation constant by using sound tube without any air spaces back of a test material,” in INTER-NOISE and NOISE-CON Congress and Conference Proceedings, pp. 1265-1268 (1998).
- [35] Y. Salissou and R. Panneton, “Wideband characterization of the complex wave number and characteristic impedance of sound absorbers,” *J. Acoust. Soc. Am.* **128**, pp. 2868-2876, (2010).
- [36] E. B. Matzke, “The three-dimensional shape of bubbles in foam-an analysis of the role of

- surface forces in three-dimensional cell shape determination,” *Am. J. Bot.*, pp. 58-80, (1946).
- [37] L. Gong, S. Kyriakides, and W.-Y. Jang, “Compressive response of open-cell foams. Part I: Morphology and elastic properties,” *Int. J. Solid. Struct.* **42**, pp. 1355-1379, (2005).
- [38] R. Panneton and X. Olny, “Acoustical determination of the parameters governing viscous dissipation in porous media,” *J. Acoust. Soc. Am.* **119**, pp. 2027-2040, (2006).
- [39] X. Olny and R. Panneton, “Acoustical determination of the parameters governing thermal dissipation in porous media,” *J. Acoust. Soc. Am.* **123**, pp. 814-824, (2008).
- [40] O. Doutres, N. Atalla, and K. Dong, “Effect of the microstructure closed pore content on the acoustic behavior of polyurethane foams,” *J. Appl. Phys.* **110**, p. 064901, (2011).
- [41] J. H. Park, K. S. Minn, H. R. Lee, S. H. Yang, C. B. Yu, S. Y. Pak, et al., “Cell openness manipulation of low density polyurethane foam for efficient sound absorption,” *J. Sound Vib.* **406**, pp. 224-236, (2017).
- [42] J.-L. Auriault, C. Boutin, and C. Geindreau, *Homogenization of coupled phenomena in heterogeneous media*, vol. 1. (Wiley Online Library, 2009).
- [43] C. Boutin and C. Geindreau, “Estimates and bounds of dynamic permeability of granular media,” *J. Acoust. Soc. Am.* **124**, pp. 3576-3593, (2008).
- [44] C. Boutin and C. Geindreau, “Periodic homogenization and consistent estimates of transport parameters through sphere and polyhedron packings in the whole porosity range,” *Phys. Rev. E* **82**, p. 036313, (2010).
- [45] Y. Achdou and M. Avellaneda, “Influence of pore roughness and poresize dispersion in estimating the permeability of a porous medium from electrical measurements,” *Phys. Fluids A-Fluid (1989-1993)* **4**, pp. 2651-2673, (1992).
- [46] M. Avellaneda and S. Torquato, “Rigorous link between fluid permeability, electrical conductivity, and relaxation times for transport in porous media,” *Phys. Fluids A-Fluid (1989-1993)* **3**, pp. 2529-2540, (1991).
- [47] D. Lafarge, “The equivalent fluid model,” *Materials and Acoustics Handbook*, pp. 153-204, (2009).
- [48] J. Allard and N. Atalla, *Propagation of sound in porous media: Modelling sound absorbing materials*, 2e. (John Wiley & Sons, 2009).
- [49] I. Malinetskaya, V.V. Mourzenko, J.-F Thovert, and P.M. Adler “Random packings of spiky particles: Geometry and transport properties,” *Phys. Rev. E* **80**, 011301(1-16), (2009).

- [50] R.A. Sampson, “On stockes’s current function,” *Philos. T. R. Soc. Lon. A* **182**, 449-518, (1891).
- [51] A. M. Kraynik, D. A. Reinelt, and F. van Swol, “Structure of random monodisperse foam,” *Phys. Rev. E* **67**, p 031403 (2003).
- [52] J. Köll and S.Hallström, “Generation of peridic stochastic foam models for numerical analysis,” *J. Cell. Plast.* **50**, pp. 37-54 (2014).